

Extracellular enzyme activity in the coastal upwelling system off Peru: a mesocosm experiment

Kristian Spilling^{1,2,*}, Jonna Piiparinen¹, Eric P. Achterberg³, Javier Arístegui⁴, Lennart T. Bach⁵, Maria T. Camarena-Gómez¹, Elisabeth von der Esch⁶, Martin A. Fischer⁷, Markel Gómez-Letona⁴, Nauzet Hernández-Hernández⁴, Judith Meyer³, Ruth A. Schmitz⁷, Ulf Riebesell³

1. Marine Research Centre, Finnish Environment Institute, Helsinki, Finland

2. Centre for Coastal Research, University of Agder, Kristiansand Norway

3. GEOMAR Helmholtz Centre for Ocean Research Kiel, Kiel, Germany

4. Instituto de Oceanografía y Cambio Global, IOCAG, Universidad de Las Palmas de Gran Canaria, Las Palmas de Gran Canaria, Spain

5. Institute for Marine and Antarctic Studies, University of Tasmania, Tasmania, Australia

6. Institute of Hydrochemistry, Chair of Analytical Chemistry and Water Chemistry, Technical University of Munich, Munich, Germany

7. Institute for General Microbiology, Christian Albrechts University Kiel, Germany

*corresponding author: kristian.spilling@syke.fi

18 Abstract

19 The Peruvian upwelling system is a highly productive ecosystem with a large oxygen minimum
20 zone (OMZ) close to the surface. Here, we carried out a mesocosm experiment off Callao, Peru,
21 with the addition of water masses from the regional OMZ collected at two different sites
22 simulating two different upwelling scenarios. Here we focus on pelagic remineralization of
23 organic matter by extracellular enzyme activity of leucine aminopeptidase (LAP) and alkaline
24 phosphatase activity (APA). After addition of the OMZ water, dissolved inorganic nitrogen (N)
25 was depleted, but the standing stock of phytoplankton was relatively high even after nutrient
26 depletion (mostly $>4 \mu\text{g chlorophyll } a \text{ L}^{-1}$). During the initial phase of the experiment, APA was
27 $0.6 \text{ nmol L}^{-1} \text{ h}^{-1}$ even though the PO_4^{3-} concentration was $>0.5 \mu\text{mol L}^{-1}$. Initially, the dissolved
28 organic phosphorus (DOP) decreased, coinciding with an increase in PO_4^{3-} concentration
29 probably linked to the APA. The LAP activity was very high with most of the measurements in
30 the range $200\text{-}800 \text{ nmol L}^{-1} \text{ h}^{-1}$. This enzyme hydrolyzes terminal amino acids from larger
31 molecules (e.g. peptides or proteins), and these high values are probably linked to the highly
32 productive, but N-limited coastal ecosystem. Also, the experiment took place during a rare
33 coastal El Niño event with higher-than-normal surface temperatures, which could have affected
34 enzyme activity. Using a non-parametric multidimensional scaling analysis (NMDS) with a
35 generalized additive model (GAM), we found that biogeochemical variables (e.g. nutrient and
36 chlorophyll *a* concentrations), phytoplankton and bacterial communities explained up to 64% of
37 the variability in APA. The bacterial community explained best the variability (34%) in LAP.
38 The high hydrolysis rates for this enzyme suggests that pelagic N remineralization, likely driven
39 by the bacterial community, supported the high standing stock of primary producers in the
40 mesocosms after N depletion.

41

42

43 Introduction

44 The Peruvian upwelling system is one of the most productive marine ecosystems in the world
45 (FAO, 2018). Its high productivity is driven by the upwelling of deep, nutrient rich water that
46 fuels primary production when reaching the sunlit surface. The primary limiting nutrient is
47 nitrogen (N), but iron (Fe) availability is also an important driver for phytoplankton biomass
48 production in addition to light (Chavez et al., 2008; Messié and Chavez, 2015). Part of the
49 phytoplankton biomass passes to higher trophic levels through grazing and predation. As the
50 upwelled water parcel is transported further offshore by Ekman transport, part of the biomass
51 settles out of the euphotic zone and is decomposed in intermediate water layers creating an
52 extensive oxygen minimum zone (OMZ; Kalvelage et al., 2013). The fate of the biomass
53 produced is consequently of great importance for higher trophic levels and for biogeochemical
54 cycles

55 After inorganic nutrients (primarily N) have been depleted, primary production in the surface
56 layer is driven by recycled production. In this process, dissolved organic matter (DOM) must
57 first be broken down into simpler forms before the DOM elements become biologically
58 available. The decomposition of DOM is not a uniform process as it is affected by both abiotic
59 and biotic variables. Extracellular enzymes hydrolyze complex dissolved organic molecules and
60 is the first step in remineralization of these DOM elements (Arnosti, 2011). Quantifying the rates
61 of pelagic remineralization is important for understanding recycled production and element
62 fluxes in the uppermost water masses. There are a range of different enzymes that are used for

hydrolyzing DOM, and two of the most studied ones are Leucine aminopeptidase (LAP) and Alkaline phosphatase (AP).

LAP hydrolyzes terminal amino acids from larger molecules (e.g. peptides or proteins) and is used extracellularly in aquatic systems by bacteria, some phytoplankton and fungi (Hoppe et al., 1988; Stoecker and Gustafson, 2003; Gutiérrez et al., 2011). It hydrolyses a broad spectrum of substrates with a free amino group, but it has preference for N-terminal leucine and related amino acids in peptides and proteins (Burley et al., 1990; Steen et al. 2015).

The AP enzyme is produced by a wide range of different organisms including aquatic bacteria and phytoplankton. Its main function is related to the hydrolysis of phosphate monoesters that separate orthophosphate (PO_4) from an organic compound (Perry, 1972; Hoppe, 2003). AP exists either as ectoenzyme (on the cell wall) or is excreted extracellularly, and for phytoplankton it has commonly been related to P-limitation in aquatic environments (Rose and Axler, 1997; Nausch, 1998). Bacterial AP activity (APA) is more complex, as some, especially particle attached bacteria, take up and use C and N from the organic molecule after hydrolysis, and may for this reason produce AP even under P replete conditions (Benitez-Nelson and Buesseler, 1999; Hoppe, 2003; Labry et al., 2016).

The ongoing warming of surface waters caused by climate change is projected to have several consequences on marine ecosystems. For example, increasing temperatures lead to a reduction in gas solubility causing a decrease in oxygen concentrations; warming will also increase thermal stratification and reduce the ventilation of the deeper ocean (Keeling et al., 2010). Both of these effects will lead to expanding OMZs with potential consequences for biogeochemical cycling (Oschlies et al., 2018). Biogeochemical cycles of nitrogen (N) and phosphorus (P) are affected

by O₂ depletions, e.g., through denitrification and sediment P release (Canfield et al., 2005).

Hence, expanding OMZs may decrease the inorganic N : P ratio in the upwelled water potentially affecting the seston (i.e. all suspended particles) stoichiometry and plankton community composition (Hauss et al., 2012; Spilling et al., 2019).

In this study, a mesocosm experiment off the coast of Peru was carried out to study the effect of ~~upwelling~~ of OMZ water to the surface, with several papers covering different aspects in this special issue. Here we were interested in the dynamics of organic matter break down. We measured the extracellular LAP and AP activities and used a statistical model to relate it to biogeochemical variables, and plankton and bacterioplankton communities. Our main aim was to understand how much of the variability in enzyme activities could be explained by biogeochemical variables (e.g. nutrient concentrations) and microbial communities.

Materials and methods

A detailed description of the mesocosm set up and collection and addition of OMZ-water can be found in Bach et al. (2020) within this special issue. Some of the basic variables such as inorganic nutrient concentration can also be found in Bach et al (2020). In short, the mesocosm bags were 2 m in diameter and extended from the surface down to 19 m depth, where the last 2 m was a conical sediment trap. Eight mesocosm bags were used and they were moored at 12.0555°S; 77.2348°W just north of Isla San Lorenzo where the water depth is ~30 m. The mesocosms were closed by attaching the sediment trap to the bottom and pulling the top above the surface on 25 Feb, 2017. The bags were regularly cleaned from the inside and outside. For a full detailed sampling and cleaning timetable see Bach et al. (2020).

~~The main aim of the experiment was to simulate different upwelling events. For this, w~~Water
(100 m³) from the oxygen minimum zone (OMZ) was collected from two locations and depths.
The first was collected from 12.028323°S; 77.223603°W from 30 m depth, and the second one
from 12.044333°S; 77.377583°W from 70 m depth. The original aim was to collect severe and
moderate OMZ signature water (differing in e.g. nitrate concentrations) from the first and second
site, respectively. This assumption was based on long-term monitoring data, however, the
chemical properties (e.g. nitrate concentration) was more similar in these water masses than
anticipated, rather reflecting low and very low OMZ signatures from site 1 and 2 respectively.
This was discovered only after the collection, and it was not technically possible to make
additional collections of OMZ water. For this reason the data presented here focus on the
temporal trend more than the difference between the two treatments, but for easier comparisons
with the other papers in this special issue we keep the same graphical interface.

To have a baseline of measured variables, the mesocosms where closed and environmental and
biological variables were determined over 10 days. After this period, the OMZ water was added
to the mesocosms in two steps on day 11 and 12 after the enclosure of the mesocosms. As the
mesocosms contain a specific volume (~54 m³), the process of adding the OMZ water started
with first removing water from the mesocosms. The water removed (~20 m³) was pumped out
from 11-12 m depth. A similar volume of OMZ water, from both collection sites, ~~wasere~~ then
pumped into four replicate mesocosms each. The OMZ water was pumped into the mesocosms
moving the input hose between 14-17 m depth. The water collected at 30 m depth was pumped
into mesocosms M1, M4, M5 and M8 having a low OMZ signature and water from 70 m depth
into mesocosms M2, M3, M6 and M7 having a very low OMZ signature. Due to the halocline at

129 12 m depth (see below), the added OMZ water was not immediately mixed throughout the
130 mesocosm bag.

131 At the site of the mesocosms, the OMZ is normally close to the surface (<10 m depth; Graco et
132 al., 2017) and consequently the bottom part of the mesocosm was low in oxygen. To keep the
133 stratification inside the mesocosm we added 69 L of concentrated brine on day 13 by carefully
134 inserting it between 12.5-17 m depth. The same procedure was repeated on day 33 when 33 L of
135 brine was added. This artificial halocline prevented complete mixing of the mesocosm and the
136 lower part of the mesocosm had a very different water chemistry compared to the upper 10 m
137 where we did all our sampling. Right after the experiment, a third addition of brine was carried
138 out to measure the total volume of the mesocosms.

139 Sampling took place every second day over a period of 50 days, and all variables were taken
140 with an integrated water sampler (HydroBios, IWS) pre-programed to fill from 0 – 10 m depth
141 and all samples consisted of this integrated samples from the upper 10 m. The samples were
142 stored dark in cool boxes and brought back to the laboratory and processed right away. Sampling
143 took place in the morning, and the samples were ~~ereere~~ usually back in the laboratory around noon.

144

145 Nutrient concentrations

146 Inorganic nutrients were determined from filtered (0.45 µm filter, Sterivex, Merck) samples
147 immediately after the water arrived in the laboratory. For the measurements, we used a
148 continuous flow analyzer (QuAatro AutoAnalyzer, SEAL Analytical) connected to a
149 fluorescence detector (FP-2020, JASCO). Phosphate (PO_4^{3-}), nitrate (NO_3^-) and nitrite (NO_2^-)

were determined colorimetrically (Murphy and Riley, 1962; Morris and Riley, 1963) and corrected with the refractive index method reported by Coverly et al. (2012). Ammonium (NH_4^+) concentrations were determined fluorometrically (K  rouel and Aminot, 1997). Dissolved inorganic nitrogen (DIN) was calculated by summing NO_3^- , NO_2^- and NH_4^+ . Further details on measurement accuracy can be found in Bach et al. (2020), where the individual DIN elements are also presented.

To measure total dissolved nitrogen (TDN) and phosphorus (TDP), the samples were first filtered through pre-combusted (5 h, 450  C) Whatman GF/F filters (pore size 0.7   m). The filtrate was collected in 50 mL acid-cleaned high-density polyethylene (HDPE) bottles and placed directly into a freezer (-20  C). Later the filtrates were thawed at room temperature over a period of 24 hours and divided in two parts. The first half was used to determine inorganic nutrient concentrations as described above. From the other half we determined the TDN and TDP concentrations. An oxidizing reagent (Oxisolv, Merck) was added, and the samples were autoclaved for 30 minutes. TDN and TDP were measured spectrophotometrically (QuAAtro, Seal Analytical). Dissolved organic nitrogen (DON) concentrations were calculated by subtracting DIN from TDN. Dissolved organic phosphorus (DOP) was calculated as the difference between TDP and PO_4^{3-} .

Fluorescent dissolved organic matter and PARAFAC analysis

Fluorescent dissolved organic matter (FDOM) was determined by measuring fluorescence in water samples with a Cary Eclipse (Agilent Technologies) spectrofluorometer, using excitation and emission slit widths of 10 nm. Wavelength ranges were set to 230-456 nm for excitation,

with 2 nm increments, and the 290-600 nm for emission with 5 nm increments. The measurements were collected into excitation-emission matrices (EEM). Blanks were measured with the same settings using ultrapure water.

Raw measurements were processed using the DOMFluor toolbox (v. 1.7; Stedmon and Bro, 2008) for Matlab (R2017a). The processing consisted of 1) blank subtraction from seawater EEMs, 2) EEMs normalization to the Raman area (RA), estimated applying the trapezoidal rule of integration on the emission scan at the 350 nm excitation wavelength in the blank EEMs, and 3) cropping of the 1st and 2nd order Rayleigh scatter bands. Inner filter correction was not performed as for the duration of the experiment the absorption coefficient at 250 nm (a_{250}) displayed values (mean \pm sd = $1.56 \pm 0.91 \text{ m}^{-1}$) well below 10 m^{-1} , above which correction is considered necessary (Stedmon and Bro, 2008).

The processed EEMs were analyzed applying a Parallel Factor Analysis (PARAFAC) using the DOMFluor toolbox. The PARAFAC model was constructed based on 125 samples (outliers were removed) and validated using split-half validation and random initialization. The resulting model consisted of 4 components (C1-C4; supplementary material Fig S1). For each of them, the fluorescence maximum (Fmax) was recorded. The identified fluorophores were compared to others found in the literature using the OpenFluor database (openfluor.lablicate.com; Murphy et al., 2014).

Phytoplankton community and chlorophyll a

193 Flow Cytometry subsamples were transferred from the IWS into 50 mL beakers and stored cool
194 in the dark until analysis max. 8 hours after sampling. Each sample (650 μ L) was analyzed with
195 an Accuri C6 flow cytometer (BD Biosciences) set to a high flow rate (i.e. 66 μ L/min).
196 Phytoplankton groups were differentiated based on the strength of the forward scatter (FSC-A),
197 the side scatter (SSC-A), the red fluorescence (FL3-A) and orange fluorescence (FL2-A) signal (
198 “A” refers to the area of the signal integral). Furthermore, we used sequential filtrations with
199 different polycarbonate filters (Whatman, pore-sizes 0.2, 0.4, 0.8, 2, 3, 5, 8 μ m) to distinguish
200 populations in the cytogram based on size. This procedure was helpful to approximate how FSC-
201 A values corresponded with size. We defined the following phytoplankton groups:
202 Synechococcus-like cells (Syn; 0.2-2 μ m), Cryptophyte-like cells (Crypto; ~90% between 2-5
203 μ m), picoeukaryotes (Peuks; 0.2-2 μ m), Nanoeukaryotes (Nano; 2-20 μ m, mostly in the lower
204 range), Microeukaryotes 1 (Mikro1; ~15-40 μ m, occasionally overlapping with Nano),
205 Microeukaryotes 2 (Mikro2; ~>40 μ m, cluster dominated by *Akashiwo sanguineum* from about
206 day 20 onward), elongated cells “chains” determined by the ratio of FSC-A to FSC-H where “H”
207 refers to the height of the forward scatter signal (details about this approach are provided in Paul
208 et al., this issue. The goal of this was to detect chain-forming diatoms which we expected to be
209 an important component of the community).

210 Samples for chlorophyll *a* (chl-*a*) determination were filtered onto GF/F filters (Whatman) and
211 flash frozen in liquid nitrogen and stored at -80 °C (or dry ice for a brief period during air
212 transfer; ~2 days) until measurement. The chl-*a* was extracted in acetone and the concentration
213 was measured using high-performance liquid chromatography calibrated against commercial
214 standards (Barlow et al., 1997). The chl-*a* autofluorescence of the phytoplankton community was
215 measured with a handheld fluorometer (AquaPen, Photon Systems Instruments) using 450 nm

216 excitation light. The photochemical efficiency was calculated based on the relationship between
 217 the variable to maximal fluorescence (F_v/F_m).

218

219 16S-rRNA gene based bacterial community determination

220 One liter of surface water obtained from the individual sampling sites was filtered through sterile
 221 Millipore Express PLUS membrane filters (polyethersulfon) with a cut-off of 0.22 μm and a
 222 diameter of 47 mm (Merck Millipore). After filtration, the filters were flash frozen in liquid
 223 nitrogen and stored at -80°C until nucleic acid extraction. Nucleic acid extraction was performed
 224 using the NucleoSpin TriPrep- Kit (Machery-Nagel) according to manufacturer's instruction
 225 with an additional step at the beginning of the extraction using a pestle to homogenize the
 226 sample.

227 Primers applied for the amplification of the bacterial 16S rRNA gene fragments were annealing
 228 to the variable region 1 and 2 and consisted of an initial standardized Illumina adapter (regular),
 229 followed by an 8 nucleotide barcode (X's), a linker region (underlined) and a primer sequence
 230 (bold). The sequences were for the forward primer Bac27 5'-
 231 AATGATACGGCGACCACCGAGATCTACACXXXXXXXXXXTATGGTAATTGTAGAGTTT
 232 **GATCCTGGCTCAG**-3' and reverse Bac338 5'-
 233 CAAGCAGAAGACGGCATACGAGATXXXXXXXXXXAGTCAGTCAGCCTGCTGCCTCCC
 234 **GTAGGAGT**-3'. The individual PCR reaction contained 100 ng of the extracted DNA. PCR
 235 conditions and purification of the amplification product were previously described (Fischer et al.
 236 2019a). The final library pool for sequencing was combined from the eluates and contained 100
 237 ng of DNA. Amplicon library sequencing was performed on a MiSeq instrument. Library

238 therefore was prepared according to the manufacturer's instructions and sequenced using the v3
239 chemistry with 2 x 300bp paired-end.

240 Reads generated with amplicon sequencing were trimmed using the trimmomatic software
241 version 0.33 (Bolger et al., 2014) as described in Fischer et al. (2019b). Briefly, reads were
242 analyzed with a sliding window of 4 bp and regions were trimmed if the average Phred score
243 (Ewing and Green, 1998; Ewing et al., 1998) within the window was below 30. Trimmed reads
244 were kept within the dataset if the forward and reverse read both survived the quality trimming
245 and were longer than 36 bp. Afterwards, 20,000 reads per sample were kept in the dataset
246 (exceptions were sample M1 on day 10 (5817 reads) and M7 on day 24 (17660 reads) for further
247 analysis.

248 Quality trimmed sequences were analyzed using MOTHUR software, version 1.35.1 (Schloss et
249 al., 2009) as described in Fischer et al. (2019a). The quality filtered and subsampled reads were
250 concatenated to 1,040,321 contiguous sequences (contigs) using the command `make.contig`.
251 Contigs were filtered for ambiguous bases, homopolymers longer than 8 bases or sequences
252 longer than 552 bases using the command `screen.seqs`. The resulting 754,310 contigs were
253 checked for redundant sequences using the command `unique.seqs` and clustered to 199,746
254 unique sequences. The sequences were consecutively aligned to a modified version of the
255 SILVA database release version 132 (Pruesse et al., 2012) containing only the hypervariable
256 regions V1 and V2 by the command `align.seqs`. Sequences not aligning in the expected region
257 were removed from the dataset using the command `screen.seqs`. The alignment was further
258 optimized by removing gap-only columns with the command `filter.seqs`. The alignment
259 contained 717,217 sequences (148,760 unique). Rare and closely related sequences were
260 clustered using the commands `unique.seqs` and `precluster.seqs`. The latter was used to cluster

sequences with up to 3 positional differences compared to larger sequence clusters together. Chimeric sequences were removed using the implemented software UCHIME (Edgar et al., 2011) using the command chimera.uchime, followed by remove.seqs leaving 551,142 sequences (29,519 unique) in the dataset. The classification of the sequences was performed against the SILVA database and was done with a bootstrap threshold of 80 %. Operational taxonomic units (OTUs) were formed using the average neighbor clustering method with the command cluster.split. A sample-by-OUT table on the 97 % level, containing 10,258 OTUs, was generated using the command make.shared. These OTUs were used for the subsequent analysis. After the removal of mitochondria, chloroplast and singletons, 3225 OTUs were retained. These OTUs were used for downstream analysis.

Extracellular enzymes

The leucine aminopeptidase (LAP) activity was determined using the method described by Stoecker and Gustafson (2003) using *L*-leucine 7-amido-4-methyl-coumarin (Leu-AMC; Sigma Aldrich) as a substrate. Leu-AMC was added to a final concentration of 500 $\mu\text{mol L}^{-1}$, which was determined in separate kinetics tests to saturate the enzyme activity. The samples (100-200 μl) were incubated in the dark at in situ surface temperature for four to six hours. The fluorescence was measured every 30-60 min with a Cary Eclipse (Agilent Technologies) spectrofluorometer using 380 nm excitation and 440 nm emission wavelengths. The results were compared with a standard curve determined using 7-amino-4-methyl-coumarin (AMC; Sigma Aldrich) dissolved in DMSO, and the LAP activity calculated by linear regression.

Measurements of alkaline phosphatase activity (APA) were conducted with 20 ml subsamples of initial/incubated seawater using 100 nmol L⁻¹ 4-methylumbelliferyl phosphate (MUF-P; Sigma-Aldrich) as the organic phosphate substrate (Ammerman, 1993). From this incubation, samples were transferred into a well plate and fluorescence was measured on a BIOTEK Microplate Reader with a Cary Eclipse (Agilent Technologies) spectrofluorometer using 355 nm excitation light and 460 nm emission detection. Following MUF-P addition, fluorescence measurements were performed at 0, 1.5, and 3 h and APA (h⁻¹) was calculated from the linear increase in fluorescence and calibrated against 4-methylumbelliferone (MUF; Sigma-Aldrich). The assays were performed and incubated in the dark. Ultrapure water (Milli-Q) blanks and paraformaldehyde-killed controls generally yielded fluorescence values similar to $t = 0$ readings.

Statistical analysis

Before comparisons of enzyme activity between the two experimental treatments (OMZ water added from two different locations) were conducted, we first constructed a cumulative value where each measured value was summed up for each sampling day. The linear regressions of the cumulative enzyme activity from the two treatments ($n = 4$) were compared with Student's t-test. In addition, the effect of biogeochemical, phytoplankton and bacterioplankton community composition to APA and LAP was determined, using the ordination scores of the first and second axis of a non-parametric multidimensional scaling (NMDS) as explanatory variables in generalized additive models (GAMs) with APA or LAP as dependent variable. The NMDS was applied separately to each group of variables: biogeochemical, phytoplankton community and

bacterioplankton community. The individual explanatory power of each MDS score was estimated with a univariate GAM. The visualization of the links was done for each explanatory variable through the prediction from the full model object, setting all other explanatory variables at their mean value. In addition, links to the scores of the biogeochemical variables and phytoplankton community NMDS were estimated with one GAM model. It was not possible to include the bacterioplankton community into this model due to the different sampling regime (lower number of samples) and this was treated with a second model. NMDS was estimated with the metaMDS function in the Vegan package (Oksanen et al., 2017), and GAMs were fitted using the gam function in the mgcv package (Wood, 2017). For explaining the deviance, an adjusted coefficient of determination (R^2) was used. An adjusted R^2 takes into account the model complexity and is more conservative than a non-adjusted R^2 .

RESULTS

Nutrients

Inorganic nutrients, dissolved inorganic nitrogen (DIN) and phosphate, were available for the two first weeks of the experiment (Fig 1). The addition of OMZ-water increased the phosphate concentrations whereas the dissolved inorganic nitrogen (DIN) was $>2 \mu\text{mol L}^{-1}$ in the mesocosms until ~~after~~ the addition of OMZ-water (days 11 and 12 of the experiment). After the addition of the OMZ-water, the DIN concentration rapidly declined and was depleted at day 15 in most mesocosms except in M3 where DIN depletion occurred a week later (day 22; Fig 1).

324 The PO_4^{3-} concentration increased after closing the mesocosm and reached $\sim 1.9 \mu\text{mol L}^{-1}$ in all
 325 mesocosms after the OMZ-water addition. There was only a slight reduction to approximately
 326 $1.5 \mu\text{mol PO}_4^{3-} \text{ L}^{-1}$ over the course of the experiment (Fig 1).

327 The dissolved organic nitrogen (DON) and phosphorus (DOP) concentrations were initially 9 –
 328 $12 \mu\text{mol L}^{-1}$ and $0.6 - 1.0 \mu\text{mol L}^{-1}$, respectively. There was no drastic change in DON with the
 329 OMZ-water addition and there was an overall decrease in DON to $6.0 - 7.9 \mu\text{mol L}^{-1}$ on day 30
 330 after which it increased somewhat again. The DOP concentrations decreased rapidly the first 8
 331 days to $0.19 - 0.32 \mu\text{mol L}^{-1}$ but increased after the OMZ-water addition and remained within 0.2
 332 $- 0.7 \mu\text{mol L}^{-1}$ interval for the rest of the experiment.

333 The PARAFAC modelling of the EEMs yielded four FDOM components (C1-C4; Fig 2 and S1).
 334 Using the OpenFluor database we identified multiple fluorophores with strong similarity
 335 ($\text{TCC}_{\text{ex-em}} > 0.95$) to our components (Table S1). Components 1 and 3 had characteristics
 336 resembling amino acid/protein-like fluorescence, whereas the fluorescence of components 2 and
 337 4 was humic-like (Table S1). All FDOM components increased sharply at day 18. This did not
 338 take place in Pacific seawater sampled outside the mesocosm where the FDOM was relatively
 339 stable throughout the experiment. After the increase at day 18, humic-like components (C2 and
 340 C4) were relatively stable but decreased slightly after day 28-30. The amino acid-like
 341 components (C1 and C3) exhibited higher variability among mesocosms, and C3 had overall
 342 higher variability throughout the experiment. Both humic-like and amino acid-like components
 343 maintained fluorescence values above the initial ones until the end of the experiment, but there
 344 were no clear differences between the treatments. However, towards the end of the experiment
 345 M1 and M2 had highest fluorescence values of C1. M1 also had highest values of C2 and C3
 346 whereas M3 had the highest values of C4 at the end of the experiment.

347

348 Chlorophyll, photochemical efficiency and phytoplankton community

349 After OMZ-water addition, the chl-*a* concentration increased from 2-4 $\mu\text{g L}^{-1}$ to 4-8 $\mu\text{g L}^{-1}$
350 except for mesocosms M3 and M4 where the increase was not as pronounced (Fig 3). The chl-*a*
351 concentration in M3 increased after day 22 to $\sim 4 \mu\text{g Chl-}a \text{ L}^{-1}$, whereas in M4 the chl-*a*
352 concentration remained low ($< 2 \mu\text{g L}^{-1}$) throughout most of the experiment (Fig 3). The
353 photochemical efficiency (F_v/F_m) was approximately 0.7 throughout the whole experiment
354 without major difference between mesocosms, except for M4 where it was consistently lower
355 (< 0.6) during the last week of experiment (Fig 3).

356 The initial community was dominated by diatoms in terms of biomass but this group gradually
357 reduced in numbers after the enclosure of the mesocosms and instead the mixotrophic
358 dinoflagellate *Akashiwo sanguineum* appeared (Fig 4). The cell counts done with the flow
359 cytometer were checked with a microscope and this was the primary species in terms of biomass
360 in the Microeukaryote 2 group (Fig 4). The exceptions were mesocosms M3 and M4 where this
361 dinoflagellate was not abundant (M4) or bloomed later (M3) and where there were more
362 Chrysophytes. In M4 there was in addition a bloom of picoeukaryotes starting after day 20 (Fig
363 4). The parallels of the same treatment did not develop in the same way in all the mesocosms,
364 and this was particularly evident from the phytoplankton community composition (Fig 4).

365

366 Bacterial community

The bacterial community was dominated by the class Alphaproteobacteria throughout the whole experiment and in all the mesocosms units, reaching values between 60 to 88% of the total sequences at day16 (Fig 5). Within Alphaproteobacteria, the *Roseobacter* lineage (genera HIMB11, *Ascidiaeihabitans*, *Amylibacter* and *Planktomarina* in M1) of the order Rhodobacterales contributed most to the bacterial community in all the mesocosms (10-55 %) in particular on day 16, except in M8 where the SAR11 Ia clade dominated the community (55% of the total sequence at day 16). The order Parvibaculales had high relative abundances (12-20% of the total sequences) in M4, M5, M6 and M7 before the OMZ-water addition (day 10) decreasing in the following week. The relative abundance of order Rickettsiales peaked at day 16 in all the mesocosms except in M8, decreasing after one week. The class Gammaproteobacteria comprised between 20 to 45% of the total relative abundance. Within Gammaproteobacteria, the order Thiomicrospirales had high relative abundance (8-17% total sequences) at day 10 in most of the mesocosms, whereas the order Cellvibrionales and order Oceanospirillales (genus *Pseudohongiella*) increased from day 24 and by the end of the experiment, respectively. In M8, the abundances of orders Thiomicrospirales and Pseudomonadales (14% of total sequences) increased at day 24. Other groups that increased in abundance in the second half of the experiment were the deltaproteobacterial orders Desulfobacterales (7-20% in M2, M3, M4 and M5) and Bdellovibrionales (5-8% in M2, M3 and M4). The order Flavobacteriales dominated within Bacteroidetes and the relative abundance ranged from 1 to 25% throughout the experiment, being generally high (10-20%) at day 10 . The flavobacterial genus *Aurantivirga* contributed > 7% in M1, M2 and M3.

Enzyme activity

390 The initial LAP activity before the OMZ-water addition was relatively low (average 359 nmol L⁻¹ h⁻¹ ± 81 nmol L⁻¹ h⁻¹ SD) but increased after the addition of OMZ-water in some of the
391 mesocosms (Fig 6). In M3 the LAP activity was high, reaching 1600 nmol L⁻¹ h⁻¹ directly after
392 the OMZ-water addition, but decreased after that. The highest overall LAP activity throughout
393 the experiment was in M7 where the LAP activity was 716 nmol L⁻¹ h⁻¹ after OMZ-water
394 addition and the average after day 16 was 657 nmol L⁻¹ h⁻¹ ± 142 nmol L⁻¹ h⁻¹ (SD). There was a
395 slight difference between the treatments in the LAP activity after the addition of the OMZ-water
396 until day 16, with the very low OMZ signature (lowest NO₃ concentration) water producing the
397 highest LAP activity (Student's t-test, p = 0.047), but this difference disappeared after day 16 (p
398 = 0.44).

400 The alkaline phosphatase activity (APA) was 0.5-0.6 nmol L⁻¹ h⁻¹ at the beginning of the
401 experiment but decreased to undetectable levels after day 30 (Fig 7). There was a noticeable drop
402 in APA after the addition of the OMZ-water, and the decrease continued gradually until day 28
403 after which the APA was very low (<0.1 nmol L⁻¹ d⁻¹). The APA was similar in all the
404 mesocosms and there was no treatment effect (p = 0.81). The exception to this was M3 where the
405 APA was lower, compared to all other mesocosms for most of the experiment (Fig 7).

406 The variability in APA was better explained by the measured variables than LAP (Fig 8). The
407 biogeochemical variables and bacterioplankton community separately explained 62% of the
408 variability in APA, whereas the phytoplankton community alone explained 57% of the
409 variability. Combining both the biogeochemical variables and the phytoplankton community
410 increased the explanatory power to 74% (bacterioplankton community not included as the
411 number of sample points were less). The variability in LAP activity was best explained by the
412 bacterioplankton community (38%) followed by biogeochemical variables (20%) and

phytoplankton community (18%). The combined biochemical variables and phytoplankton community explained 28% of the LAP variability.

DISCUSSION

After the closure and addition of OMZ-water there was rapid phytoplankton growth in the upper 5 m of the mesocosms, with low light conditions limiting primary production deeper down (Bach et al., 2020). The DIN concentrations were depleted around day 18 coinciding with an increase in several of the FDOM components (both amino acid-like and humic-like components), also matching the end of the phytoplankton bloom. There was, however, relatively constant and low export of carbon out from the mesocosms (Bach et al., 2020) and at the same time relatively high Chl-*a* concentration (mostly $>4 \mu\text{g chl-}a \text{ L}^{-1}$) under conditions with depleted DIN (Fig 3). In addition, the photochemical efficiency was overall relatively high (>0.5) throughout the experiment suggesting regenerated primary production driven by recycling of nutrients. The measured hydrolysis rates, particularly LAP, indicated that extracellular enzyme activity plays an important role for this recycled production.

The main aim of this study was to relate the biogeochemical and microbial community to the extracellular enzyme activity and a more detailed description of the temporal development and biomass comparison of microbial groups will be presented elsewhere in this special issue (e.g. Bach et al., 2020; Schulz et al 2021; Chen et al 2022; Paul et al 2022). Among phytoplankton, diatoms are typically dominating following upwelling events (Anabalón et al., 2016), whereas

434 dinoflagellates tend to become more dominant after establishment of stratification (Margalef et
435 al., 1979). This was also seen in our mesocosm as the dinoflagellate *Akashiwo sanguinea*, a
436 mixotrophic species that may form red tides (Jeong et al., 2005; Badylak et al., 2014), ~~which that~~
437 quickly appeared ~~in some mesocosms in most mesocosm after OMZ water was added~~ with some
438 exceptions. In M3 it appeared a little later ~~than in most mesocosms~~ and in M4 it did not bloom at
439 all. Interestingly these two mesocosms had a higher concentration of cryophytes and M4 had
440 additionally a bloom event of picoeukaryotes. Being mixotrophic, *A. sanguinea* is known to prey
441 on smaller species (Jeong et al., 2005) and lower grazing pressure could be the reason for the
442 bloom of picoeukaryotes in M4.

443 The bacterial community composition changed during the experiment but without clear treatment
444 effects. The dominant bacterial groups were the class Alphaproteobacteria, (Parvibaculales,
445 SAR11 subclade Ia, Roseobacter clade and Rickettsiales), class Gammaproteobacteria (SAR116
446 clade, Cellvibrionales, Oceanospirillales and SUP05 clade) and to lesser extent the class
447 Deltaproteobacteria (Desulfobacterales) and class Bacteroidia (order Flavobacteriales). SAR11
448 subclade Ia, Roseobacter clade, SAR116 clade, SUP05 clade and Desulfobacterales are known to
449 utilize inorganic and organic sulfur components such as hydrogen sulfide (H₂S), sulfate (SO₄)
450 and dimethylsulfoniopropionate (DMSP) metabolites for their metabolic requirements (Nowinski
451 et al., 2019) and are coupled with the nitrogen cycle (Schunck et al., 2013). Specifically, the
452 sulfur-oxidizing SUP05 oxidizes H₂S coupled with the nitrate reduction and potentially produces
453 nitrite (Shah et al., 2017), whereas Desulfobacterales play an important role in N₂ fixation (Gier
454 et al., 2016). These bacterial taxa associated with the sulfur cycle are typically found in the OMZ
455 regions (Pajares et al., 2020). We observed a temporal shift in the bacterial community through
456 the experiment changing between sulfur-oxidizing (SUP05) and sulfate-reducing

(Desulfobacterales) bacteria, probably linked to the nitrate availability, i.e. more DIN at the enclosure of the mesocosms and thus more relative abundance of SUP05. We also observed a shift within phytoplankton-associated bacteria (*Roseobacter* lineage, Gammaproteobacteria, and Flavobacteriales) that likely responded to the availability of DOM supply during the experiment (Buchan et al 2014, Chafee et al 2017). The high relative abundance of Flavobacteriales and genera from the *Roseobacter* lineage on days 10 and 16, respectively, coincided with the increase in chl-*a* and high LAP activity until day 16. Positive correlations have been observed between chl-*a*, Bacteroides and Deltaproteobacteria and LAP during phytoplankton blooms (Shi et al 2019). However, we do not have gene expression data and cannot make any firm conclusion about the connection between these groups and production of LAP.

The temporal shift in the bacterial community indicates niche partitioning between bacterial taxa that assimilate different organic substrates or inorganic sulfur components, produced during phytoplankton bloom events or from sulfidic events (Schunck et al., 2013; Callbeck et al., 2018; Nowinski et al., 2019). Our results support previous studies that have demonstrated the important role of the sulfur cycle in shaping the bacterial community composition in poorly oxygenated waters (Schunck et al., 2013; Aldunate et al., 2018). It is worth noting that the conditions in the bottom of the mesocosms were sub-oxic and there might have been a clear depth gradient in the bacterial community that was not picked up by our integrated 0-10 m sampling.

Overall, there was a treatment effect of the different OMZ waters on the LAP activity, with higher LAP in the very low OMZ signature addition, but this effect was only observed right after the addition of the OMZ-water. There were also slightly higher NO₃ concentrations in this water (Bach et al., 2020). However, this difference in both DIN and LAP was relatively small and disappeared a week after the OMZ water addition, most likely because the collected OMZ-water

wasere more similar between the two locations than anticipated, with relatively similar concentrations of DIN. Although there were differences between individual mesocosms in terms of the plankton community structure, there were no clear differences between treatments, and we can conclude that the availability of nutrients by itself can shift the LAP production.

The LAP activity in our study was very high (~10-times higher compared with most literature data). In a comparable study but further offshore in Peru, the LAP activity was 20 – 65 nmol L⁻¹ h⁻¹ in surface waters (Maßmig et al., 2020). Further to the south, in Chile (30° 30.80' S), values up to 230 nmol L⁻¹ h⁻¹ have been recorded, with a clear seasonal cycle linked to upwelling events (Gutiérrez et al., 2011). With most of our data ranging between 200 – 800 nmol L⁻¹ h⁻¹ it is clear that these LAP activities are linked to the upwelling, which is more intense near the coast and also more constant at the study site compared with sites further south. The enzyme activity in sediments can be up to three orders of magnitude higher than what we found (Hoppe et al., 2002), and an order of magnitude higher values have been observed in a eutrophic, salt-water lake (Song et al., 2019). The high LAP activities are likely a reflection of the high microbial activity in the Peruvian upwelling system. The experiment was also taking place during a rare coastal El Niño event (Garreaud, 2018), with anomalous higher surface temperatures (20-22 °C), which could be a reason for the high values we recorded as LAP activity is known to increase with temperature (Christian and Karl, 1995).

There was also some loss of N due to denitrification, estimated to 0.2-4.2 nmol N₂ L⁻¹ h⁻¹ during the experiment (Schulz et al 2021). For comparison, the LAP activity suggested an average of 417 nmol L⁻¹ h⁻¹ hydrolyzation of N-containing compounds, but this should be seen as the maximal potential rather than the actual rate. The use of fluorescently labelled substrates for measuring extracellular activity is a proxy method that has some drawbacks. The primary one is

that the molecular structure of the substrate used is never equivalent to the high molecular weight DOM in the water. This means that the measured hydrolysis rates could be an overestimation of the actual hydrolysis rates of DOM (e.g. Arnosti, 2011). The primary benefit of the method is that it is straightforward and has been in widespread use for decades, which means that comparisons with other ecosystems is possible, and for our purpose, we use it for better understanding how much of the variability can be explained by the other measured variables.

Considering the APA, the most interesting aspect was that it was measurable in the beginning of the experiment at high PO_4^{3-} concentration. This high APA activity at high PO_4^{3-} concentration has been observed in deep oceans (Hoppe and Ullrich, 1999; Baltar et al 2016). Baltar et al. (2016) also observed an increase in APA in experiments amended with organic matter suggesting the activity of APA was linked to organic matter supply, independently of the PO_4^{3-} concentration. This could be due to bacterial APA, which is more complex than for phytoplankton, in that it can be linked to the hydrolysis and acquisition of C (Hoppe, 2003). In our experiment, the initial decrease in DOP and increase in PO_4^{3-} concentrations indicates that P released by the-AP hydrolysis was of DOP added to the PO_4^{3-} pool. This suggests that APA was not used for P acquisition.

It is known that APA stays suspended and active for a long time in marine environments, and cell-free APA was reduced by only 25% over 16 days in the experiment by Thomson et al. (2019). If this enzyme is viable for this long, it suggests that there was no new production of AP after the closure of the mesocosms, which is supported by the dilution effect of adding the OMZ-water. In that case, the disappearance of the initial AP took 30 days.

The hydrolysis rates of AP were relatively low compared with most published data, probably linked to the clear surplus of PO_4^{3-} . It is worth ~~to~~ noting, however, that we were most likely not measuring the maximal potential hydrolysis rates as substrate addition was relatively low (100 nmol L^{-1}) and would likely have been higher with more added substrate. This could be the reason for the apparent discrepancy between the measured hydrolysis rates and the change in the PO_4^{3-} and DOP pools during the 10 first days of the experiment. During this time there was a decrease of approximately $0.5 \text{ } \mu\text{mol DOP L}^{-1}$ and an increase of $0.6 \text{ } \mu\text{mol PO}_4^{3-} \text{ L}^{-1}$, suggesting an actual hydrolysis rate of $2.0\text{-}2.5 \text{ nmol L}^{-1} \text{ h}^{-1}$ (assuming $500\text{-}600 \text{ nmol}$ over 10 days). This is a factor 3-4 higher compared with the initially measured APA of $\sim 0.6 \text{ nmol L}^{-1} \text{ h}^{-1}$.

The statistical model that we applied was better at explaining the variability in APA compared with the LAP activity. APA gradually decreased during the initial phase of the experiment to undetectable levels after the middle of the experiment. Any correlation does not mean causality and the higher coefficient of determination is probably rather a reflection of the clear temporal development in APA. If the AP was produced before the closure of the mesocosm and slowly degraded as discussed above, any connection with the biogeochemical or plankton community ~~was~~ ere likely due to unrelated temporal development; for example, the DIN also decreased over time.

For the LAP activity the overall explanatory power by the biogeochemical and plankton community composition was less than for APA, but interestingly the bacterioplankton community composition clearly explained the variability better (38%) than the combined biogeochemical and phytoplankton community (28%). Considering that the bacterial community was not sampled as frequently as the biogeochemical variables and flow cytometer counts, we suspect that the explanatory power would have increased with more frequent sampling. It is

likely that bacteria were producing the LAP activity and some taxa are more reliant on enzyme production for nutrient acquisition than others (Ramin and Allison, 2019). Some dinoflagellates are also known to produce LAP and most of the mesocosms with high dinoflagellate biomass except M4. However, the phytoplankton community only explained 18% of the variability in LAP activity, and these dinoflagellates were likely not producing any substantial amount of this enzyme.

In conclusion, there was measurable APA at the start of the experiment, but this gradually declined to undetectable levels in all the mesocosms midway (~30 days) in the experiment. With high concentrations of PO_4^{3-} , low APA is not surprising, and AP is a relatively slowly degrading enzyme that could have been fully dissolved and produced before the closure of the mesocosms. Our statistical model explained better the variability of APA (74%) compared with LAP activity, probably due to the clear temporal development of APA that was likely independent of some of the other temporal trends such as decreasing DIN. We found very high levels of LAP activity (mostly in the range $200 - 800 \text{ nmol L}^{-1} \text{ h}^{-1}$), which is an order of magnitude higher than most literature data. This is probably linked to the upwelling supporting high levels of microbial activity in combination with the general DIN limitation in the coastal Peruvian upwelling. The bacterioplankton community composition explained best the variability of LAP activity (38%) compared with the combined biochemical and phytoplankton community model (28%). With more than 50% of the variability unaccounted for, we are still missing important pieces of the puzzle understanding the variability in LAP activity. The high hydrolysis rates for LAP suggests that pelagic N remineralization supported the relatively high standing stock of primary producers (mostly $>4 \mu\text{g chl-}a \text{ L}^{-1}$) in the mesocosms after N depletion.

570

571 Data availability

572 All data will be made available on the permanent repository www.pangaea.de after publication.

573 The DNA sequencing data will be submitted to NCBI SRA (in prep).

574

575 Author contribution

576 Samples were taken by KS, JP, JA, LB, EvdE, MF, NHH, JM and UR. In addition to the
577 sampling crew, further data analysis was conducted by MTCG and MGL. UR developed the
578 experimental design and sampling strategy and coordinated the mesocosm campaign. All co-
579 authors contributed to the data interpretation. KS wrote the manuscript with contributions from
580 all co-authors.

581

582 ACKNOWLEDGEMENTS

583 The experiment was funded through the German Research Foundation (DFG) project:
584 Collaborative Research Centre SFB 754 Climate1074 Biogeochemistry Interactions in the
585 Tropical Ocean. Additional funding came from the Academy of Finland (decision 259164; KS
586 and JP), the EU project AQUACOSM (UR) under grant No. 731065 of the European Union's
587 Horizon 2020 research and innovation programme, the Leibniz Award 2012 of the German
588 Research Foundation (UR) and the Helmholtz International Fellow Award 2015 (JA). This study
589 also used SYKE marine research infrastructure as a part of the Finnish FINMARI consortium.

The publication of sequencing data was approved by the Peruvian Ministry of Production with respect to the access and benefit sharing regulations of the Nagoya protocol.

We thank all participants of the KOSMOS-Peru 2017 study for assisting in mesocosm sampling and maintenance in particular: Andrea Ludwig, Jana Meyer, Jean-Pierre Bednar, Gabriela Chavez, Susanne Feiersinger, Peter Fritsche, Paul Stange, Anna Schukat and Michael Krudewig. We are particularly thankful to the staff of IMARPE for their support during the planning, and to the Marina de Guerra del Perú, the Dirección General de Capitanías y Guardacostas and the Club Náutico Del Centro Naval for their great support. The NMDS plots and GAM models were produced by Dr. Riina Klais-Peets at EcoStat ltd.

REFERENCES

Aldunate, M., De la Iglesia, R., Bertagnolli, A. D., and Ulloa, O.: Oxygen modulates bacterial community composition in the coastal upwelling waters off central Chile, Deep Sea Research Part II: Topical Studies in Oceanography, 156, 68-79, 2018.

Ammerman, J.: Microbial cycling of inorganic and organic phosphorus in the water column, Handbook of methods in aquatic microbial ecology, 1, 649-660, 1993.

Anabalón, V., Morales, C., González, H., Menschel, E., Schneider, W., Hormazabal, S., Valencia, L., and Escribano, R.: Micro-phytoplankton community structure in the coastal

609 upwelling zone off Concepción (central Chile): Annual and inter-annual fluctuations in a highly
610 dynamic environment, *Prog Oceanogr*, 149, 174-188, 2016.

611 Arnosti, C.: Microbial extracellular enzymes and the marine carbon cycle, *Ann Rev Mar Sci*, 3,
612 401-425, 2011.

613 Bach, L. T., Alvarez-Fernandez, S., Hornick, T., Stuhr, A., and Riebesell, U.: Simulated ocean
614 acidification reveals winners and losers in coastal phytoplankton, *PloS one*, 12, e0188198, 2017.

615 Bach, L. T., Paul, A. J., Boxhammer, T., Esch, E. v. d., Graco, M., Schulz, K. G., Achterberg, E.,
616 Aguayo, P., Aristegui, J., Ayon, P., Banos, I., Bernales, A., Boegeholz, A. S., Chavez, F., Chen,
617 S.-M., Doering, K., Filella, A., Fischer, M., Grasse, P., Haunost, M., Hennke, J., Hernandez-
618 Hernandez, N., Hopwood, M., Igarza, M., Kalter, V., Kittu, L., Kohnert, P., Ledesma, J.,
619 Lieberum, C., Lischka, S., Loescher, C., Ludwig, A., Mendoza, U., Meyer, J., Meyer, J.,
620 Minutolo, F., Cortes, J. O., Piiparinen, J., Sforna, C., Spilling, K., Sanchez, S., Spisla, C., Sswat,
621 M., Moreira, M. Z., and Riebesell, U.: Factors controlling plankton productivity, particulate
622 matter stoichiometry, and export flux in the coastal upwelling system off Peru, *Biogeosciences*
623 17: 4831-4852, 2020.

624 Badylak, S., Philips, E. J., and Mathews, A. L.: *Akashiwo sanguinea* (Dinophyceae) blooms in a
625 sub-tropical estuary: an alga for all seasons, *Plankt Benthos Res*, 9, 147-155, 2014.

626 Barlow, R., Cummings, D., and Gibb, S.: Improved resolution of mono-and divinyl chlorophylls
627 a and b and zeaxanthin and lutein in phytoplankton extracts using reverse phase C-8 HPLC, *Mar*
628 *Ecol Prog Ser*, 161, 303-307, 1997.

629 Benitez-Nelson, C. R., and Buesseler, K. O.: Variability of inorganic and organic phosphorus
630 turnover rates in the coastal ocean, *Nature*, 398, 502-505, 1999.

631 Bolger, A. M., Lohse, M., and Usadel, B.: Trimmomatic: a flexible trimmer for Illumina
632 sequence data, *Bioinformatics*, 30, 2114-2120, 2014.

633 Buchan, A., G. R. LeClerc, C. A. Gulvik, and J. M. González. 2014. Master recyclers: Features
634 and functions of bacteria associated with phytoplankton blooms. *Nat. Rev. Microbiol.* 12: 686–
635 698. doi:10.1038/nrmicro3326.

636 Burley, S. K., David, P. R., Taylor, A., and Lipscomb, W. N.: Molecular structure of leucine
637 aminopeptidase at 2.7-Å resolution, *Proc Natl Acad Sci*, 87, 6878-6882, 1990.

638 Canfield D., Kristensen E., and Thamdrup B.: *Aquatic geomicrobiology*. Elsevier, 2005.

639 Callbeck, C. M., Lavik, G., Ferdelman, T. G., Fuchs, B., Gruber-Vodicka, H. R., Hach, P. F.,
640 Littmann, S., Schoffelen, N. J., Kalvelage, T., and Thomsen, S.: Oxygen minimum zone cryptic
641 sulfur cycling sustained by offshore transport of key sulfur oxidizing bacteria, *Nature Com*, 9, 1-
642 11, 2018.

643 Chafee M, Fernández-Guerra A, Buttigieg PL, Gerds G, Eren AM, Teeling H, Amann RI (2017)
644 Recurrent patterns of microdiversity in a temperate coastal marine environment. *The ISME J*
645 12:237

646 Chavez, F. P., Bertrand, A., Guevara-Carrasco, R., Soler, P., and Csirke, J.: The northern
647 Humboldt Current System: Brief history, present status and a view towards the future, *Prog*
648 *Oceanogr*, 79, 95-105, 2008.

649 Chen, S.-M., Riebesell, U., Schulz, K. G., von der Esch, E., Achterberg, E. P., and Bach, L. T.:
650 Temporal dynamics of surface ocean carbonate chemistry in response to natural and simulated
651 upwelling events during the 2017 coastal El Niño near Callao, Peru, *Biogeosciences*, 19, 295–
652 312, 2022.

653 Christian J.R., Karl D.M.: Bacterial ectoenzymes in marine waters: activity ratios and
654 temperature responses in three oceanographic provinces. *Limnol Oceanogr*, 40:1042-1049, 1995.

655 Coverly, S., Kérouel, R., and Aminot, A.: A re-examination of matrix effects in the segmented-
656 flow analysis of nutrients in sea and estuarine water, *Analytica chimica acta*, 712, 94-100, 2012.

657 Edgar, R. C., Haas, B. J., Clemente, J. C., Quince, C., and Knight, R.: UCHIME improves
658 sensitivity and speed of chimera detection, *Bioinformatics*, 27, 2194-2200, 2011.

659 Ewing, B., and Green, P.: Base-calling of automated sequencer traces using phred. II. Error
660 probabilities, *Genome Res*, 8, 186-194, 1998.

661 Ewing, B., Hillier, L., Wendl, M. C., and Green, P.: Base-calling of automated sequencer traces
662 using Phred. I. Accuracy assessment, *Genome Res*, 8, 175-185, 1998.

663 FAO: The state of world fisheries and aquaculture, Food and Agriculture Organization of the
664 United Nations, Rome, 223 pp., 2018.

665 Fischer, M. A., Güllert, S., Refai, S., Künzel, S., Deppenmeier, U., Streit, W. R., and Schmitz, R.
666 A.: Long-term investigation of microbial community composition and transcription patterns in a
667 biogas plant undergoing ammonia crisis, *Microb Biotechnol*, 12, 305-323, 2019a.

668 Fischer, M. A., Ulbricht, A., Neulinger, S. C., Refai, S., Waßmann, K., Künzel, S., and Schmitz-
 669 Streit, R. A.: Immediate effects of ammonia shock on transcription and composition of a biogas
 670 reactor microbiome, *Front Microbiol*, 10, 2064, 2019b.

671 Garreaud, R. D.: A plausible atmospheric trigger for the 2017 coastal El Niño, *International J*
 672 *Climatol*, 38, e1296-e1302, 2018.

673 Gier, J., Sommer, S., Löscher, C. R., Dale, A. W., Schmitz-Streit, R., and Treude, T.: Nitrogen
 674 fixation in sediments along a depth transect through the Peruvian oxygen minimum zone,
 675 *Biogeosciences*, 13, 4065-4080, 2016.

676 Graco, M. I., Purca, S., Dewitte, B., Castro, C. G., Morón, O., Ledesma, J., Flores, G., and
 677 Gutiérrez, D.: The OMZ and nutrient features as a signature of interannual and low-frequency
 678 variability in the Peruvian upwelling system, *Biogeosciences*, 14, 4601-4617, 2017.

679 Gutiérrez, M., Pantoja, S., Tejos, E., and Quiñones, R.: The role of fungi in processing marine
 680 organic matter in the upwelling ecosystem off Chile, *Mar Biol*, 158, 205-219, 2011.

681 Hauss, H., Franz, J. M., and Sommer, U.: Changes in N: P stoichiometry influence taxonomic
 682 composition and nutritional quality of phytoplankton in the Peruvian upwelling, *J Sea Res*, 73,
 683 74-85, 2012.

684 Hoppe, H.-G., Kim, S.-J., and Gocke, K.: Microbial decomposition in aquatic environments:
 685 combined process of extracellular enzyme activity and substrate uptake, *Appl. Environ.*
 686 *Microbiol.*, 54, 784-790, 1988.

687 Hoppe, H.-G., Arnosti, C., and Herndl, G.: Ecological significance of bacterial enzymes in the
 688 marine environment, in: *Enzymes in the Environment: Activity, Ecology, and Applications*,
 689 edited by: Burns R. G and Dick R. P), Marcel Dekker, New York, 73-107, 2002.

690 Hoppe, H.-G.: Phosphatase activity in the sea, *Hydrobiol*, 493, 187-200, 2003.

691 Jeong, H. J., Du Yoo, Y., Park, J. Y., Song, J. Y., Kim, S. T., Lee, S. H., Kim, K. Y., and Yih,
 692 W. H.: Feeding by phototrophic red-tide dinoflagellates: five species newly revealed and six
 693 species previously known to be mixotrophic, *Aquat Microb Ecol*, 40, 133-150, 2005.

694 Kalvelage, T., Lavik, G., Lam, P., Contreras, S., Arteaga, L., Löscher, C. R., Oschlies, A.,
 695 Paulmier, A., Stramma, L., and Kuypers, M. M.: Nitrogen cycling driven by organic matter
 696 export in the South Pacific oxygen minimum zone, *Nature Geosci*, 6, 228-234, 2013.

697 Keeling, R. F., Körtzinger, A., and Gruber, N.: Ocean deoxygenation in a warming world, *Ann*
 698 *Rev Mar Sci*, 2, 199-229, 2010.

699 Kérouel, R., and Aminot, A.: Fluorometric determination of ammonia in sea and estuarine waters
 700 by direct segmented flow analysis, *Mar Chem*, 57, 265-275, 1997.

701 Labry, C., Delmas, D., Youenou, A., Quere, J., Leynaert, A., Fraisse, S., Raimonet, M., and
 702 Ragueneau, O.: High alkaline phosphatase activity in phosphate replete waters: The case of two
 703 macrotidal estuaries, *Limnol Oceanogr*, 61, 1513-1529, 2016.

704 Margalef, R., Estrada, M., and Blasco, D.: Functional morphology of organisms involved in red
 705 tides, as adapted to decaying turbulence, in: *Toxic dinoflagellate blooms*, edited by: Taylor, D.
 706 L., and Seliger, H. H., Elsevier-North Holland, Amsterdam, 89-94, 1979.

707 Maßmig, M., Lüdke, J., Krahmann, G., and Engel, A.: Bacterial degradation activity in the
 708 eastern tropical South Pacific oxygen minimum zone, *Biogeosciences*, 17, 215-230, 2020.

709 Messié, M., and Chavez, F. P.: Seasonal regulation of primary production in eastern boundary
 710 upwelling systems, *Prog Oceanogr*, 134, 1-18, 2015.

711 Morris, A., and Riley, J.: The determination of nitrate in sea water, *Analytica Chimica Acta*, 29,
 712 272-279, 1963.

713 Murphy, J., and Riley, J. P.: A modified single solution method for the determination of
 714 phosphate in natural waters, *Analytica Chimica Acta*, 27, 31-36, 1962.

715 Murphy, K. R., Stedmon, C. A., Wenig, P., and Bro, R.: OpenFluor—an online spectral library of
 716 auto-fluorescence by organic compounds in the environment, *Analytical Meth*, 6, 658-661, 2014.

717 Nausch, M.: Alkaline phosphatase activities and the relationship to inorganic phosphate in the
 718 Pomeranian Bight (southern Baltic Sea), *Aquat Microb Ecol*, 16, 87-94, 1998.

719 Nowinski, B., Motard-Côté, J., Landa, M., Preston, C. M., Scholin, C. A., Birch, J. M., Kiene, R.
 720 P., and Moran, M. A.: Microdiversity and temporal dynamics of marine bacterial
 721 dimethylsulfoniopropionate genes, *Env Microbiol*, 21, 1687-1701, 2019.

722 Oksanen, J., Blanchet, F.G., Kindt, R., Legendre, P.M.P.R., Minchin, P.R., O'hara, R.B.,
 723 Simpson, G., Solymos, P., Henry, M. and Stevens, H.: Ordination methods, diversity analysis
 724 and other functions for community and vegetation ecologists, *Vegan: Community Ecol Package*,
 725 5-26, 2017. Oschlies, A., Brandt, P., Stramma, L., and Schmidtko, S.: Drivers and mechanisms
 726 of ocean deoxygenation, *Nature Geosci*, 11, 467-473, 2018.

727 Pajares, S., Varona-Cordero, F., and Hernández-Becerril, D. U.: Spatial Distribution Patterns of
 728 Bacterioplankton in the Oxygen Minimum Zone of the Tropical Mexican Pacific, *Microb Ecol*,
 729 2020.

730 Paul, A. J., Bach, L. T., Arístegui, J., von der Esch, E., Hernández-Hernández, N., Piiparinen, J.,
 731 Ramajo, L., Spilling, K., and Riebesell, U.: Upwelled plankton community modulates surface
 732 bloom succession and nutrient availability in a natural plankton assemblage, *Biogeosciences*, 19,
 733 5911–5926, 2022.

734 Perry, M.: Alkaline phosphatase activity in subtropical Central North Pacific waters using a
 735 sensitive fluorometric method, *Mar Biol*, 15, 113-119, 1972.

736 Pruesse, E., Peplies, J., and Glöckner, F. O.: SINA: accurate high-throughput multiple sequence
 737 alignment of ribosomal RNA genes, *Bioinformatics*, 28, 1823-1829, 2012.

738 Rose, C., and Axler, R. P.: Uses of alkaline phosphatase activity in evaluating phytoplankton
 739 community phosphorus deficiency, *Hydrobiol*, 361, 145-156, 1997.

740 Ramin K.I., and Allison S.D.: Bacterial tradeoffs in growth rate and extracellular enzymes. *Front*
 741 *Microbiol*, 10: 2956, 2019.

742 Schloss, P. D., Westcott, S. L., Ryabin, T., Hall, J. R., Hartmann, M., Hollister, E. B.,
 743 Lesniewski, R. A., Oakley, B. B., Parks, D. H., and Robinson, C. J.: Introducing mothur: open-
 744 source, platform-independent, community-supported software for describing and comparing
 745 microbial communities, *Appl Env Microbiol*, 75, 7537-7541, 2009.

746 Schulz, K. G., Achterberg, E. P., Arístegui, J., Bach, L. T., Baños, I., Boxhammer, T., Erler, D.,
 747 Igarza, M., Kalter, V., Ludwig, A., Löscher, C., Meyer, J., Meyer, J., Minutolo, F., von der Esch,
 748 E., Ward, B. B., and Riebesell, U.: Nitrogen loss processes in response to upwelling in a
 749 Peruvian coastal setting dominated by denitrification – a mesocosm approach, *Biogeosciences*,
 750 18, 4305–4320, 2021.

751 Schunck, H., Lavik, G., Desai, D. K., Großkopf, T., Kalvelage, T., Löscher, C. R., Paulmier, A.,
 752 Contreras, S., Siegel, H., and Holtappels, M.: Giant hydrogen sulfide plume in the oxygen
 753 minimum zone off Peru supports chemolithoautotrophy, *PloS One*, 8, e68661, 2013.

754 Shah, V., Chang, B. X., and Morris, R. M.: Cultivation of a chemoautotroph from the SUP05
 755 clade of marine bacteria that produces nitrite and consumes ammonium, *ISME J*, 11, 263-271,
 756 2017.

757 Song, C., Cao, X., Zhou, Y., Azzaro, M., Monticelli, L. S., Maimone, G., Azzaro, F., La Ferla,
 758 R. and Caruso, G.: Nutrient regeneration mediated by extracellular enzymes in water column and
 759 interstitial water through a microcosm experiment. *Sci Tot Env* 670, 982-992, 2019.

760 Spilling, K., Camarena-Gómez, M.-T., Lipsewers, T., Martinez-Varela, A., Díaz-Rosas, F.,
 761 Eronen-Rasimus, E., Silva, N., von Dassow, P., and Montecino, V.: Impacts of reduced inorganic
 762 N: P ratio on three distinct plankton communities in the Humboldt upwelling system, *Mar Biol*,
 763 166, 114, 2019.

764 Steen, A.D., Vazin, J.P., Hagen, S.M., Mulligan, K.H. and Wilhelm, S.W.: Substrate specificity
 765 of aquatic extracellular peptidases assessed by competitive inhibition assays using synthetic
 766 substrates, *Aquat Microb Ecol*, 75, 271-281, 2015.

767 Stedmon, C. A., and Bro, R.: Characterizing dissolved organic matter fluorescence with parallel
768 factor analysis: a tutorial, *Limnology and Oceanography: Methods*, 6, 572-579, 2008.

769 Stoecker, D. K., and Gustafson, D. E.: Cell-surface proteolytic activity of photosynthetic
770 dinoflagellates, *Aquat Microb Ecol*, 30, 175-183, 2003.

771 Thomson, B., Wenley, J., Currie, K., Hepburn, C., Herndl, G. J., and Baltar, F.: Resolving the
772 paradox: continuous cell-free alkaline phosphatase activity despite high phosphate
773 concentrations, *Mar Chem*, 214, 103671, 2019.

774 Wood, S. N.: *Generalized additive models: an introduction with R*, CRC press, New York, 2017.

775

776

777

778

779 Figure legends

780

781 Fig 1. The concentration of dissolved inorganic nitrogen (DIN), phosphate (PO_4^{3-}), dissolved
782 organic nitrogen (DON) and phosphorus (DOP). The red and blue color are the mesocosm bags
783 with addition of water with low (closer to shore) and very low (further offshore) oxygen
784 minimum zone (OMZ) signature, respectively. The green dashed lines denote the time of OMZ

water addition. Pacific denotes measurements from water collected next to, but outside of the mesocosms.

Fig 2. The fluorescence dissolved organic matter (FDOM) components (C1-C4) during the experiment. The red and blue color are the mesocosm bags with addition of water with low (closer to shore) and very low (further offshore) oxygen minimum zone (OMZ) signature, respectively. The green dashed lines denote the time of OMZ water addition. Pacific denotes measurements from water collected next to, but outside of the mesocosms.

Fig 3. The Chlorophyll-*a* (Chl-*a*) concentration (upper graph) and the photochemical efficiency (lower graph). The red and blue color are the mesocosm bags with addition of water with low (closer to shore) and very low (further offshore) oxygen minimum zone (OMZ) signature, respectively. The green dashed lines denote the time of OMZ water addition. Pacific denotes measurements from water collected next to, but outside of the mesocosms.

Fig 4. Development of the main groups of phytoplankton enumerated by flow cytometry. The red and blue color are the mesocosm bags with addition of water with low (closer to shore) and very low (further offshore) oxygen minimum zone (OMZ) signature, respectively. The green dashed

lines denote the time of OMZ water addition. Pacific denotes measurements from water collected next to, but outside of the mesocosms.

Fig 5. The bacterial community composition in the 8 mesocosms taken at different time points. In the upper row are mesocosms with water from low OMZ signature (30 m depth) and in the second row with very low OMZ signature (70 m depth). The Y-axis indicates the relative abundance of the bacterial taxa. Only the groups that contributed more than 0.5 % of the total sequences are included and the rest are grouped as “Other Bacteria”. The classification was performed mainly in class, order and genus levels. The abbreviations indicate the main class levels: Alphaproteobacteria (orange shades), Gammaproteobacteria (blue-pink shades), Deltaproteobacteria (green shades), and Bacteroidia (yellow shades) .

Fig 6. The leucine aminopeptidase (LAP) activity. The red and blue color are the mesocosm bags with addition of water with low (closer to shore) and very low (further offshore) oxygen minimum zone (OMZ) signature, respectively. The green dashed lines denote the time of OMZ water addition. Pacific denotes measurements from water collected next to, but outside of the mesocosms.

825 Fig 7. The alkaline phosphatase activity (APA). The red and blue color are the mesocosm bags
826 with addition of water with low (closer to shore) and very low (further offshore) oxygen
827 minimum zone (OMZ) signature, respectively. The green dashed lines denote the time of OMZ
828 water addition.

829

830

831 Fig 8. Non-parametric multidimensional scaling (NMDS) plots for biochemical, phytoplankton
832 community and bacterioplankton community (upper row). From the NMDS scores, generalized
833 additive models (GAMs) were made (lower two rows) where we used alkaline phosphatase
834 activity (APA) and leucine aminopeptidase (LAP) as dependent variables. The output scores
835 (mds1 and mds2) of the NMDS are depicted in the lower two rows.

836

837

838

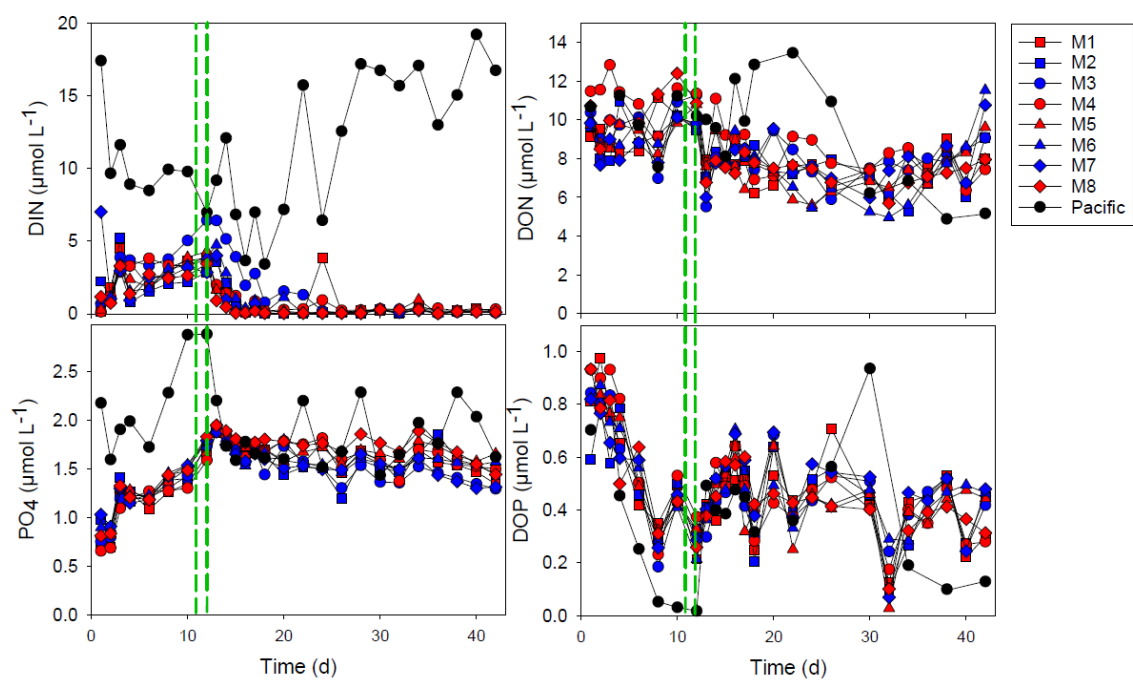


FIG 1

839
840
841
842

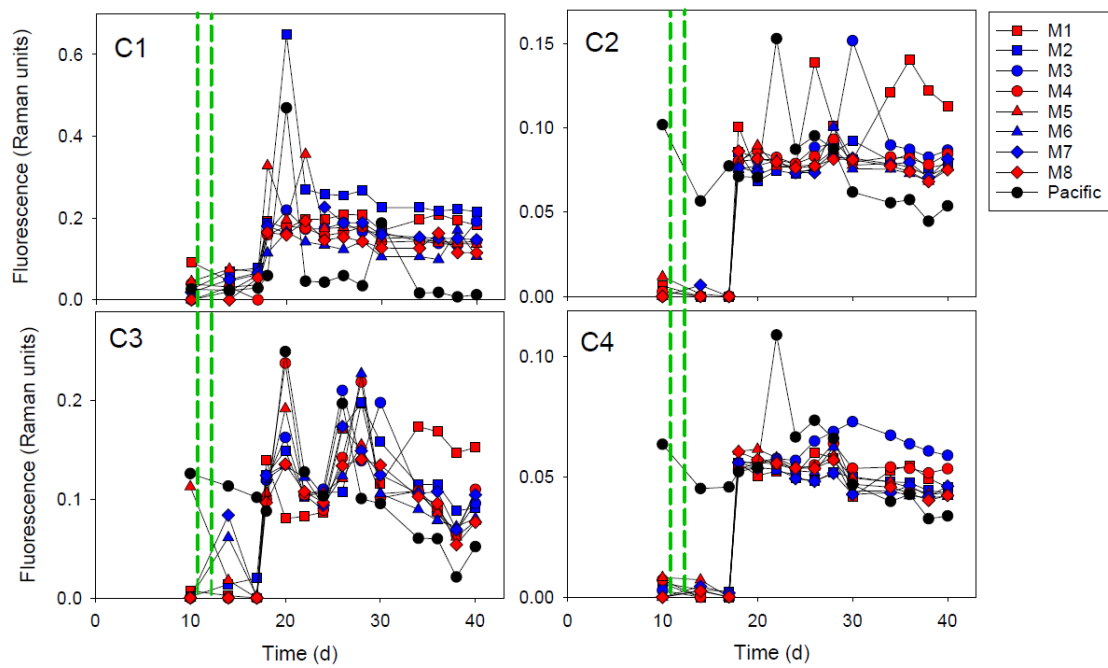


FIG 2

843
844

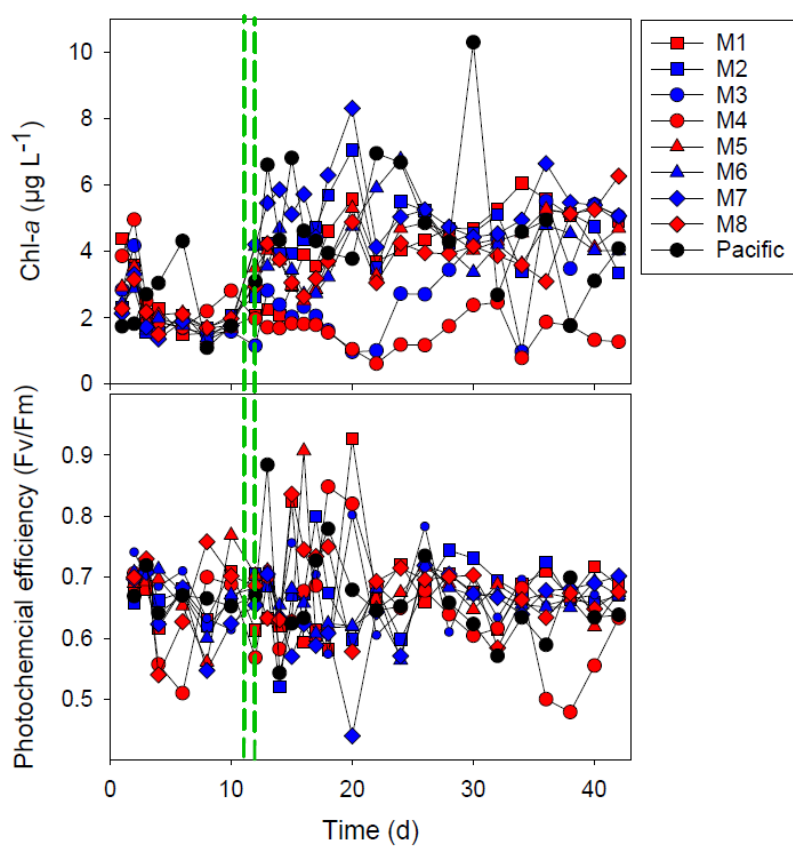


FIG 3

845
846

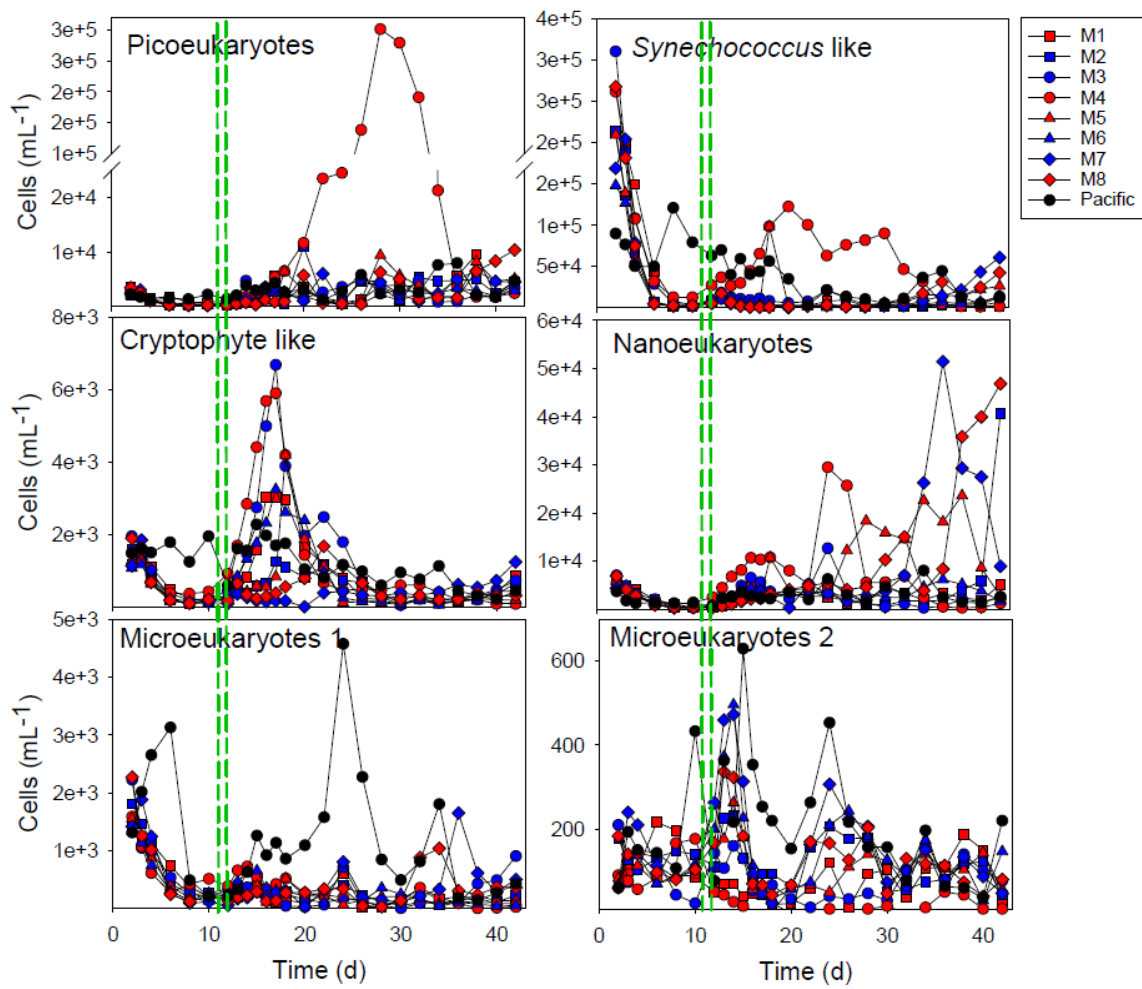
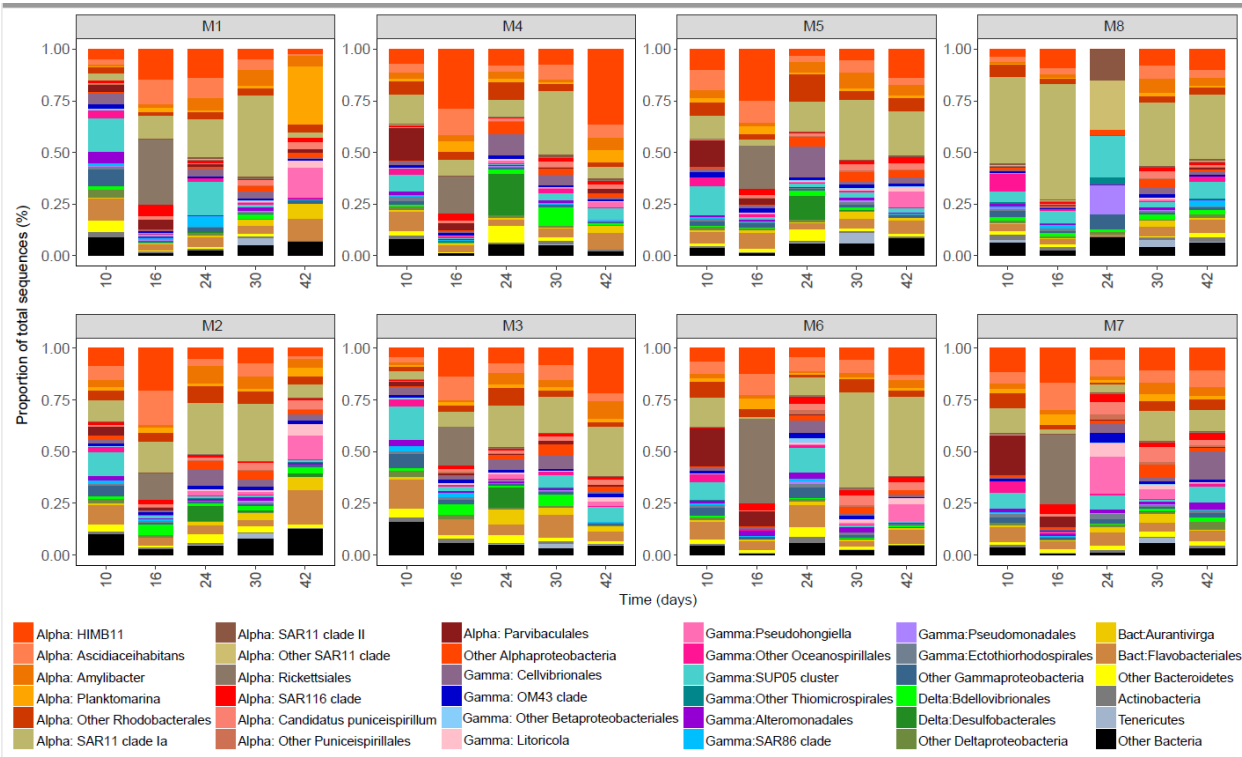


FIG 4

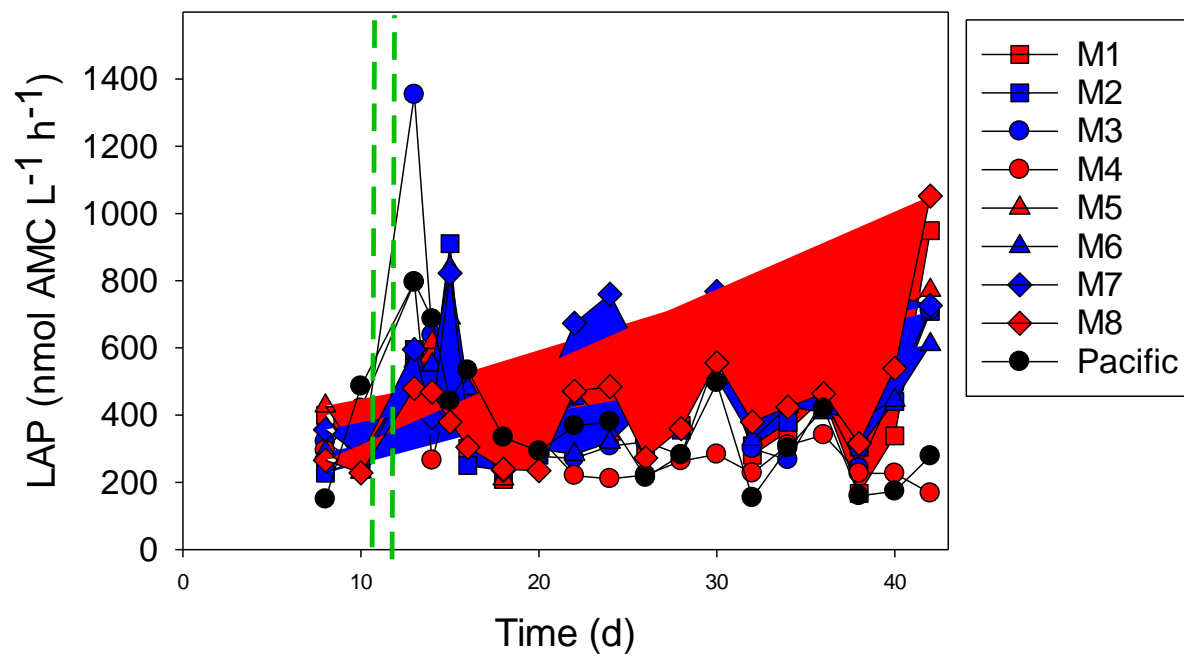
850



851

852 FIG 5

853

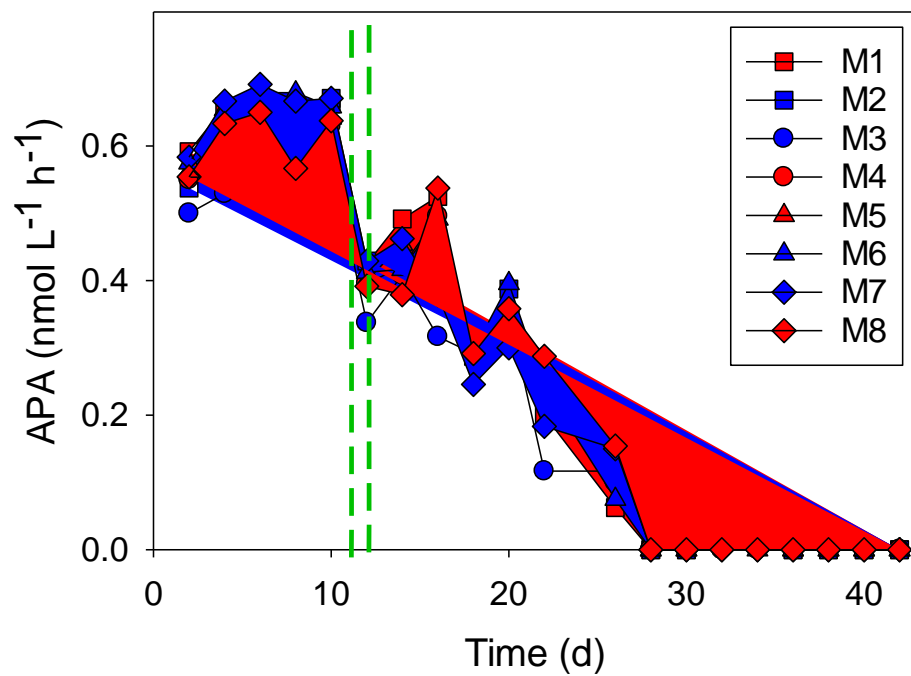


854

855 Fig 6

856

857



858

859 Fig 7

860

